Improvements and limitations of Mie λ-6 potential for prediction of saturated and compressed liquid viscosity

Richard A. Messerly

Thermodynamics Research Center, National Institute of Standards and Technology, Boulder, Colorado, 80305

Michelle C. Anderson

Thermodynamics Research Center, National Institute of Standards and Technology, Boulder, Colorado, 80305

S. Mostafa Razavi

Department of Chemical and Biomolecular Engineering, The University of Akron, Akron, Ohio, 44325-3906

J. Richard Elliott

Department of Chemical and Biomolecular Engineering, The University of Akron, Akron, Ohio, 44325-3906

Abstract

Over the past decade, the Mie λ-6 (generalized Lennard-Jones) potential has grown in popularity due to its improved accuracy for predicting vapor-liquid coexistence densities and pressure compared to the traditional Lennard-Jones 12-6 potential. This manuscript explores the hypothesis that greater accuracy in characterizing the coexistence properties may lead to greater accuracy for viscosity predictions. Four united-atom force fields are considered in detail: the Transferable Potentials for Phase Equilibria (TraPPE-UA and the recently developed TraPPE-2) model of Siepmann and coworkers, the Transferable Anisotropic Mie (TAMie) model of Gross and coworkers, the fourth generation anisotropic-united-atom (AUA4) model of Ungerer and coworkers, and the model of Potoff and coworkers.

Equilibrium molecular dynamics simulations are analyzed using the Green-Kubo method for viscosity characterization. Simulations are performed for linear alkanes with two to

Email addresses: `richard.messerly@nist.gov` (Richard A. Messerly), `michelle.anderson@nist.gov` (Michelle C. Anderson), `sr87@zips.uakron.edu` (S. Mostafa Razavi), `elliot1@uakron.edu` (J. Richard Elliott)

twenty-two carbons and branched alkanes with four to eight carbons. Simulation conditions follow the saturated liquid from reduced temperatures of 0.5 to 0.85 and along the 293 K isotherm in the dense liquid region.

In general, the more accurate force fields for coexistence properties do indeed predict viscosity more accurately. For saturated liquids, both Mie-based potential models (Potoff and TAMie) provide roughly 10 % accuracy for linear alkanes, while deviations are between 20 and 50 % for TraPPE-UA. For branched alkanes, the performance is slightly diminished, but Potoff still provides roughly 15 to 20 % accuracy, while the TAMie force field results in deviations of 20 to 40 %, and TraPPE-UA has deviations of approximately 25 to 60 %. The AUA4 deviations are 10 to 20 % for ethane and 30 to 60 % for 2,2-dimethylpropane, the only compounds tested with the AUA4 force field. The TraPPE-2 deviations for ethane are similar to those using the original TraPPE force field, namely, between 10 and 20 %. The percent deviations for each compound and force field tend to increase with decreasing temperature, with the exception of the Potoff deviations for propane, which are nearly constant to the triple point temperature.

For compressed liquids, the Mie-based potential models perform better once again than the Lennard-Jones-based force fields, but tend to over estimate the viscosity at very high densities. As the Potoff and TAMie models also tend to over estimate the pressure at high densities, a fortuitous cancellation of errors leads to predictions of viscosity with respect to pressure that are accurate to within about 10 %. The comparison with experimental viscosity data is limited to pressures below 200 MPa for most normal and branched alkanes. However, accurate predictions are obtained for propane near 1000 MPa with the Potoff force field.

1. Introduction

The design of efficient and reliable technical processes requires accurate estimates of thermophysical properties. Shear viscosity (η) is an important property for characterizing flow, e.g., sizing pumps, assessing flow assurance in fossil fuel recovery, and lubricating bearings in tribological applications. There are primarily three different means by which shear viscosity values are obtained: experimental measurement, semi-empirical prediction models, and molecular simulation (molecular dynamics, MD). Significant limitations exist for each of these methods.

For example, experimental measurements can be expensive, time-consuming, and challenging at extreme temperatures (T) and pressures (P) [1, 2] Experimental data tend to be distributed among several prototypes of linear, branched, ring, and polar molecules, with many gaps among a homologous series. Most experimental data are available below 200 MPa, while tribological applications may require estimates at pressures as high as 1000 MPa. Flow assurance applications are generally at pressures below 200 MPa, but at temperatures of 423 to 523 K. The ever expanding conditions of interest and economic constraints on new measurements foster increased research in predictive methods.

The National Institute of Standards and Technology (NIST) Reference Fluid Properties (REFPROP) database software provides "reference quality" viscosity correlations for experimentally well-studied compounds (around 100 species) [3]. Most compounds, however, do not have sufficient *reliable* experimental data covering a wide range of temperatures, pressures, and densities (ρ) for developing "reference quality" correlations. These less-studied compounds require predictive methods that pool together data from several related molecular species.

Semi-empirical prediction models are typically not reliable over the industrially relevant ranges of $P\rho T$ [4]. For example, corresponding states methods are recommended for vapors, dense fluids, and high temperature liquids. These methods rely on the similarity of trends in the properties relative to reference compounds, e.g., methane and n-octane. Corresponding states methods are less reliable for more complex molecular structures,

e.g., branched compounds. Typical compilations indicate that deviations from experiment may vary by 5 to 50 %, with little guidance about when to expect lower or higher accuracy.

For low temperature liquids, group contribution schemes are favored, but these tend to extrapolate poorly when applied to compounds or conditions outside the training set. More recent advances such as machine learning [5, 6] and entropy scaling [7] have shown great promise in prediction of historically challenging properties, such as viscosity, thermal conductivity, and surface tension. However, machine learning relies on large amounts of experimental data and often suffers from dubious extrapolation. While entropy scaling has a stronger theoretical basis, it typically requires a reliable reference viscosity and an adequate equation-of-state, which may not be readily available for the compound of interest.

As an alternative to experiment and semi-empirical prediction models, molecular simulation is an attractive means for estimating viscosity. However, there are two fundamental challenges impeding the use of molecular simulation as a mainstream chemical engineering tool for viscosity prediction. The first challenge is that obtaining reproducible results is more difficult for transport properties, such as viscosity, than for thermodynamic properties. Recently, a "Best Practices Guide" was developed to address this challenge, namely, to improve reproducibility of viscosity estimates [8]. We apply these "Best Practices" and address some outstanding issues mentioned therein.

The second challenging aspect of obtaining accurate simulation estimates is that viscosity is extremely sensitive to the force field. In addition to the strong dependence on the non-bonded interactions, the bonded potential plays a much greater role for viscosity than for thermodynamic properties. For example, varying the torsional potential has a significant impact on viscosity [9], while vapor-liquid coexistence is relatively unaffected [10]. Therefore, the ability to predict viscosities with molecular simulation requires both robust methods and adequate force fields.

We investigate the accuracy of four force fields, namely, Transferable Potentials for

4

Phase Equilibria (TraPPE-UA, also referred to simply as TraPPE [11, 12, 13]), Transferable Anisotropic Mie (TAMie) [14, 15], Potoff [16, 17], and fourth generation anisotropic-united-atom (AUA4) [18, 19]. Each force field is a variation of the united-atom (UA) Mie λ-6 (generalized Lennard-Jones, LJ) model, a popular class designed for the engineering purpose of predicting thermophysical properties. However, the suitability of these force fields for quantitative viscosity prediction, especially at high pressures, has been widely debated in the literature.

In particular, depending on the compound structure and state conditions, some studies suggest that UA LJ 12-6 models (e.g., TraPPE) are inadequate for estimating viscosities and recommend the use of anisotropic-united-atom (AUA) or all-atom (AA) models for this purpose [20, 21, 22, 23, 24]. Despite AA force fields being more physically realistic, most do not provide quantitatively reliable viscosities and some AA force fields are even less accurate than their simpler UA counterparts [20, 24]. Furthermore, considering the significant increase in computational cost of AA simulations, two promising alternatives have been investigated to improve the less-expensive UA and AUA force fields, namely, the Mie λ-6 potential and/or modified torsional models.

For example, Nieto-Draghi et al. demonstrate systematic improvement in viscosity prediction for the AUA4 model by increasing the torsional barriers [9, 19]. The primary advantage of this approach is that the torsional barriers do not typically impact thermodynamic properties and, thus, the non-bonded parameters do not need to be re-optimized. Alternatively, the UA Mie λ-6 model has been shown to accurately predict saturated liquid viscosity ($\eta_{\text{liq}}^{\text{sat}}$) without significant degradation of other vapor-liquid saturation properties [25], i.e., saturated liquid density ($\rho_{\text{liq}}^{\text{sat}}$), saturated vapor density ($\rho_{\text{vap}}^{\text{sat}}$), and saturated vapor pressure ($P_{\text{vap}}^{\text{sat}}$). However, Ewen et al. purport that the Potoff (UA Mie 16-6) force field performs poorly when predicting compressed liquid viscosities ($\eta_{\text{liq}}^{\text{comp}}$) for n-hexadecane at a temperature of 423 K [24].

Hoang et al. demonstrate that including viscosity data in the force field development can improve the identification of a unique set of transferable Mie λ-6 parameters,

while simultaneously improving viscosity predictions [26]. By contrast, the force fields compared in the present work were optimized solely with vapor-liquid coexistence data, i.e., dynamic properties, such as viscosity, were not included in their parameterization. Notwithstanding the potential benefits of including viscosity as a property of interest during force field development, we assess the accuracy of TraPPE-UA, TAMie, Potoff, and AUA4 for estimating viscosity as they currently stand, including their torsional potential models. While the Potoff and TAMie force fields have shown considerable promise in predicting static properties (in particular, $P_{\mathrm{vap}}^{\mathrm{sat}}$), their ability to predict dynamic properties has yet to be thoroughly investigated (we are aware of only three viscosity values that have been reported using the Potoff force field for normal or branched alkanes [24]).

The outline for the present work is the following. Section 2 explains the force fields, simulation methodology, and data analysis. Section 3 presents the simulation results for each force field, compound, and state point studied. Section 4 discusses some important observations and limitations. Section 5 recaps the primary conclusions from this work.

2. Methods

2.1. Force fields

A united-atom (UA) or anisotropic-united-atom (AUA) representation is used for each compound studied, i.e., normal and branched alkanes are represented with CH_3, CH_2, CH, and C sites. UA models assume that the UA interaction site is that of the carbon atom, while AUA models assume that the AUA interaction site is shifted away from the carbon atom and towards the hydrogen atom(s). Note that TraPPE and Potoff are UA force fields while TraPPE-2 (a recent improvement of TraPPE for ethane and ethylene), AUA4, and TAMie are AUA force fields.

The results presented in this work are obtained using fixed bond-lengths. Each force field utilizes a 0.154 nm bond-length for bonds not involving a CH_3 site. The anisotropic-united-atom models (TAMie, AUA4, and TraPPE-2) use a slightly longer "effective" bond-length for CH_3 bonds (see Table 1). While the TAMie force field modifies only the terminal CH_3 sites, AUA4 displaces the interaction location of CH_2 and CH sites as well. For

6

simplicity, we only utilize the AUA4 force field with compounds that are composed exclusively of CH_3 and C interaction sites, i.e., ethane and 2,2-dimethylpropane.

Table 1: Effective bond-lengths in units of nm for terminal (CH_3) UA or AUA interaction sites. Empty table entries for TraPPE-2 [13] denote that the force field does not contain the corresponding interaction site type. Empty table entries in AUA4 [18] arise because this force field uses a more complicated construction than the simple effective bond-length approach. Specifically, AUA4 requires CH_2 and CH interaction sites that are not along the C-C bond axis.

Bond	TraPPE, Potoff	TAMie	AUA4	TraPPE-2
CH_3-CH_3	0.154	0.194	0.1967	0.230
CH_3-CH_2	0.154	0.174	–	–
CH_3-CH	0.154	0.174	–	–
CH_3-C	0.154	0.174	0.1751	–

The same angle and dihedral potentials are used for each force field. Angular bending interactions are evaluated using a harmonic potential:

$$u^{\text{bend}} = \frac{k_\theta}{2} \left(\theta - \theta_0 \right)^2 \tag{1}$$

where u^{bend} is the bending energy, θ is the instantaneous bond angle, θ_0 is the equilibrium bond angle (see Table 2), and k_θ is the harmonic force constant with $k_\theta / k_B = 62500 \, \text{K/rad}^2$ for all bonding angles, where k_B is the Boltzmann constant.

Table 2: Equilibrium bond angles (θ_0) [12]. CH_i and CH_j represent CH_3, CH_2, CH, or C sites.

Bending sites	θ_0 (degrees)
CH_i-CH_2-CH_j	114.0
CH_i-CH-CH_j	112.0
CH_i-C-CH_j	109.5

Dihedral torsional interactions are determined using a cosine series:

$$u^{\text{tors}} = c_0 + c_1[1 + \cos\phi] + c_2[1 - \cos 2\phi] + c_3[1 + \cos 3\phi] \tag{2}$$

where u^{tors} is the torsional energy, ϕ is the dihedral angle and c_n are the Fourier constants listed in Table 3.

Table 3: Fourier constants (c_n/k_{B}) in units of K [12]. CH_i and CH_j represent CH_3, CH_2, CH, or C sites.

Torsion sites	c_0/k_{B}	c_1/k_{B}	c_2/k_{B}	c_3/k_{B}
CH_i-CH_2-CH_2-CH_j	0.0	355.03	-68.19	791.32
CH_i-CH_2-CH-CH_j	-251.06	428.73	-111.85	441.27
CH_i-CH_2-C-CH_j	0.0	0.0	0.0	461.29
CH_i-CH-CH-CH_j	-251.06	428.73	-111.85	441.27

Non-bonded interactions between sites located in two different molecules or separated by more than three bonds within the same molecule are calculated using a Mie λ-6 potential (of which the Lennard-Jones, LJ, 12-6 is a subclass) [27]:

$$u^{\text{vdw}}(\epsilon, \sigma, \lambda; r) = \left(\frac{\lambda}{\lambda - 6}\right)\left(\frac{\lambda}{6}\right)^{\frac{6}{\lambda-6}} \epsilon \left[\left(\frac{\sigma}{r}\right)^{\lambda} - \left(\frac{\sigma}{r}\right)^{6}\right] \tag{3}$$

where u^{vdw} is the van der Waals interaction, σ is the distance (r) where $u^{\text{vdw}} = 0$, $-\epsilon$ is the energy of the potential at the minimum $\left(\text{i.e., } u^{\text{vdw}} = -\epsilon \text{ and } \frac{\partial u^{\text{vdw}}}{\partial r} = 0 \text{ for } r = r_{\text{min}}\right)$, and λ is the repulsive exponent.

The non-bonded Mie λ-6 force field parameters for TraPPE, TraPPE-2, Potoff, AUA4, and TAMie are provided in Table 4. Notice that Potoff and TAMie utilize Mie 16-6 and Mie 14-6 potentials, respectively, whereas TraPPE, TraPPE-2, and AUA4 are LJ 12-6 based force fields. As the repulsive barrier is steeper for larger values of λ, the Potoff potential is the "hardest" at close distances. The TAMie potential is "softer" than Potoff, but still more repulsive than the TraPPE, TraPPE-2, and AUA4 models.

Note that TAMie implements an ethane-specific set of CH_3 parameters. TraPPE and TraPPE-2 are both considered in this study for ethane. Also, Potoff reports a "generalized"

Table 4: Non-bonded (intermolecular) parameters for TraPPE [11, 12] (and TraPPE-2 [13]), Potoff [16, 17], AUA4 [18, 19], and TAMie [14, 15] force fields. The "short/long" Potoff CH and C parameters are included in parentheses. The ethane-specific parameters for TAMie are included in parentheses.

United-atom	TraPPE (TraPPE-2)			Potoff (S/L)		
	ϵ/k_B (K)	σ (nm)	λ	ϵ/k_B (K)	σ (nm)	λ
CH_3	98 (134.5)	0.375 (0.352)	12	121.25	0.3783	16
CH_2	46	0.395	12	61	0.399	16
CH	10	0.468	12	15 (15/14)	0.46 (0.47/0.47)	16
C	0.5	0.640	12	1.2 (1.45/1.2)	0.61 (0.61/0.62)	16
	AUA4			TAMie		
CH_3	120.15	0.3607	12	136.318 (130.780)	0.36034 (0.36463)	14
CH_2	86.29	0.3461	12	52.9133	0.40400	14
CH	50.98	0.3363	12	14.5392	0.43656	14
C	15.04	0.244	12	–	–	–

and "short/long" (S/L) CH and C parameter set. The "short" and "long" parameters are implemented when the number of carbons in the backbone is ≤ 4 and > 4, respectively. Due to their superior accuracy, we only provide results for the Potoff S/L parameter set.

Non-bonded parameters between two different site types (i.e., cross-interactions) are determined using Lorentz-Berthelot combining rules [28] for ϵ and σ and an arithmetic mean for the repulsive exponent λ (as recommended in Reference 16):

$$\epsilon_{ij} = \sqrt{\epsilon_{ii}\epsilon_{jj}} \tag{4}$$

$$\sigma_{ij} = \frac{\sigma_{ii} + \sigma_{jj}}{2} \tag{5}$$

$$\lambda_{ij} = \frac{\lambda_{ii} + \lambda_{jj}}{2} \tag{6}$$

where the ij subscript refers to cross-interactions and the subscripts ii and jj refer to same-site interactions.

2.2. Simulation set-up

Viscosity estimates can be obtained from both equilibrium molecular dynamics (EMD) and non-equilibrium molecular dynamics (NEMD) simulations. The "Best Practices Guide" is currently limited to EMD methods and purports that NEMD might be necessary for high viscosities (greater than 0.02 Pa-s). One purpose of the present work is to demonstrate that, by applying these guidelines, EMD can also provide meaningful estimates for highly viscous systems.

Equilibrium molecular dynamics simulations are performed using GROMACS version 2018 with "mixed" (single and double) precision [29]. GROMACS is compiled using GNU 7.3.0, OpenMPI enabled, and GPU support disabled. Approximately three-fourths of the simulations are run using Linux 4.4.0-112-generic x86_64 on an Intel(R) Xeon(R) CPU E5-2699 v4 @ 2.20GHz machine while the remaining one-fourth are run using Linux 4.15.0-22-generic x86_64 on an Intel(R) Xeon(R) CPU E5-2450 0 @ 2.10GHz machine. Example GROMACS input files (.top, .gro. and .mdp) with corresponding shell and python scripts for preparing, running, and analyzing simulations are provided as Supporting Information.

Simulation specifications are provided in Table 5. Note that each force field utilizes a 1.4 nm non-bonded cut-off distance (r_c), with the exception of Potoff which employs a 1.0 nm cut-off (as recommended in Reference 16) except for certain compounds (see Section 4.3). Analytical non-bonded tail corrections for internal energy and pressure are applied in all cases (see Section 4.9 of Reference [29]). Note that GROMACS neglects the long-range contribution from the repulsive ($r^{-\lambda}$) term as it is several orders of magnitude smaller than the attractive (r^{-6}) contribution. With this simplification, the energy and pressure corrections are proportional to $\epsilon\sigma^6 r_c^{-3}$. Section 4.3 provides a detailed analysis of the cut-off length.

Section 4.2 demonstrates finite-size effects are typically negligible for a simulation with 400 molecules. For most systems, 1 ns is a sufficient production time, while longer simulations are required for the more viscous systems, e.g., 16 ns for 2,2,4-trimethylpentane

10

at 1000 MPa. Sections SI.IV and SI.V of Supporting Information investigate, respectively, the sensitivity of our results to the production time and constrained bonds. To validate our methods, a comparison with other reference simulation values [30, 31, 9] is provided in Section SI.VII of Supporting Information.

Table 5: General simulation specifications.

Time-step (fs)	2
Equilibration time (ns)	1
Production time (ns)	1, 2, 4, 8, or 16
Cut-off length (nm)	1.4 (1.0 for Potoff)
Tail-corrections	U and P
Constrained bonds	LINCS [32, 33]
LINCS-order	8
Number of molecules	400

When η is desired at a prescribed T and P, six simulation stages are required: energy minimization, NPT equilibration, NPT production, energy minimization, NVT equilibration, and NVT production. When η is desired at a prescribed T and ρ, the NPT stages are unnecessary and only three simulation stages are required: energy minimization, NVT equilibration, and NVT production. Note that the final production stage simulations are always performed using the NVT ensemble [8]. Details regarding the thermostats and barostats employed are provided in Section SI.III of Supporting Information.

We utilize 30 to 60 independent replicates to improve the precision and to provide more rigorous estimates of uncertainty [8, 34]. To ensure independence between replicates, the entire series of simulation stages are repeated for each replicate. Each energy minimization stage starts with a different pseudo-random configuration while the initial velocities are also randomized for each equilibration stage.

We investigate two different classes of viscosity, namely, saturated liquid viscosity

11

($\eta_{\text{liq}}^{\text{sat}}$) and compressed liquid viscosities ($\eta_{\text{liq}}^{\text{comp}}$) at a temperature of 293 K. Saturated liquid viscosities are estimated by performing NVT ensemble simulations at the saturation temperature (T^{sat}) and saturated liquid density ($\rho_{\text{liq}}^{\text{sat}}$). The simulation densities correspond to the REFPROP $\rho_{\text{liq}}^{\text{sat}}$, which is admittedly not necessarily the same as the force field $\rho_{\text{liq}}^{\text{sat}}$. This point is discussed in greater detail in Section 4.

Two different simulation protocols are implemented for estimating compressed liquid viscosities. Specifically, we perform simulations with each force field either at the same ρ or the same P. For the purpose of comparing the accuracy of force fields, these two methods are essentially equivalent. From a practical standpoint, estimating η at a given P requires performing preliminary NPT ensemble simulations to determine the corresponding box size.

2.3. Data analysis

We implement the Green-Kubo "time-decomposition" analysis to extract viscosity from EMD simulations. We refer the interested reader to References 8 and 34 for details regarding this method. In brief, the Green-Kubo integral is computed with respect to time according to

$$\eta(t) = \frac{V}{k_{\text{B}} T N_{\text{reps}}} \sum_{n=1}^{N_{\text{reps}}} \int_0^t dt' \, \langle \tau_{\alpha\beta,n}(t') \tau_{\alpha\beta,n}(0) \rangle_{t_0,\alpha\beta} \tag{7}$$

where t is time, V is volume, N_{reps} is the number of independent replicate simulations, α and β are x, y, or z Cartesian coordinates, $\tau_{\alpha\beta,n}$ is the α-β off-diagonal atomic stress tensor element for the nth replicate, and $\langle \cdots \rangle_{t_0,\alpha\beta}$ denotes an average over time origins (t_0) and the τ_{xy}, τ_{xz}, and τ_{yz} tensor elements. Equation 7 averages several (between 30 and 60) independent replicate simulations, twelve different time-origins, and all three unique off-diagonal stress tensor components to improve numerical precision. Furthermore, $\tau_{\alpha\beta,n}$ is recorded every 6 fs (3 time-steps) for accurate integration of Equation 7.

The "true" viscosity, i.e., the infinite-time-limit viscosity, is obtained by evaluating Equation 7 as $t \rightarrow \infty$. However, the long-time tail of the Green-Kubo integral is often quite

12

noisy and does not converge smoothly. For this purpose, we fit the "running integral" to a double-exponential function

$$\eta(t) = A\alpha\tau_1 \left(1 - \exp\left(-t/\tau_1\right)\right) + A(1 - \alpha)\tau_2 \left(1 - \exp\left(-t/\tau_2\right)\right) \tag{8}$$

where A, α, τ_1, and τ_2 are fitting parameters and $\eta^\infty = A\alpha\tau_1 + A(1 - \alpha)\tau_2$ is the infinite-time-limit viscosity.

Since the Green-Kubo "running integral" suffers from extreme fluctuations at long times, Equation 8 is fit by minimizing a weighted sum-squared error objective function. Weights are equal to the inverse of the standard deviation (σ_η) of the replicate simulations. The time dependence of σ_η is modeled with Bt^b, where B and b are fitting parameters.

Despite weighting the data by σ_η, it can be challenging to obtain good fits of Equation 8 when all the data are included. For this reason, data are excluded where $\sigma_\eta > 0.4 \times \eta^\infty$ [8, 34]. Occasionally, this heuristic results in a cut-off that is too short, in particular for systems with slow dynamics, which also leads to very poor fits. In such cases, it is necessary to modify the heuristic, e.g., exclude data where $\sigma_\eta > 0.8 \times \eta^\infty$. As erroneously large fluctuations also exist at very short times, only data for $t > 3$ ps are included in the fitting of Equation 8 [8, 34].

The uncertainty in η^∞ is obtained by bootstrap re-sampling. Specifically, the fitting process described previously is repeated hundreds of times using randomly selected subsets of replicate simulations. Furthermore, each bootstrap repetition uses a randomly selected long-time cut-off between $0.35 \times \eta^\infty$ and $0.45 \times \eta^\infty$ to account for uncertainty in the $0.4 \times \eta^\infty$ heuristic. A 95 % confidence interval is obtained from the distribution of bootstrap estimates for η^∞. An example of this process is provided in Section SI.VI of Supporting Information.

3. Results

Seven normal and seven branched alkanes of varying chain-length and degree of branching are simulated in this study. We only consider compounds with available REF-PROP equations-of-state and viscosity correlations [3]. Specifically, we simulate ethane

[35, 36], propane [37, 38], *n*-butane [39, 40], *n*-octane [41, 42], *n*-dodecane [43, 44], *n*-hexadecane [45, 46], *n*-docosane [45, 47], 2-methylpropane [48, 49], 2-methylbutane [48, 47], 2-methylpentane [48, 47], 3-methylpentane [50, 47], 2,2-dimethylpropane [48, 47], 2,3-dimethylbutane [50, 47], and 2,2,4-trimethylpentane [51, 47].

Each compound was simulated using the TraPPE and Potoff S/L force fields. Potoff "short" parameters are employed for 2-methylpropane, 2-methylbutane, 2,2-dimethylpropane, and 2,3-dimethylbutane while Potoff "long" parameters are utilized for 2-methylpentane, 3-methylpentane, and 2,2,4-trimethylpentane. Since we are not aware of any TAMie parameters for C sites, 2,2-dimethylpropane and 2,2,4-trimethylpentane were not simulated using the TAMie force field. Only ethane and 2,2-dimethylpropane were simulated with AUA4. See Section SI.II of Supporting Information for a comprehensive list of all systems studied.

Sections 3.1 and 3.2 present results for saturated liquid viscosities ($\eta_{\text{liq}}^{\text{sat}}$) and compressed liquid viscosities ($\eta_{\text{liq}}^{\text{comp}}$), respectively. In both sections, the *n*-alkane results are followed by the branched alkane results. Simulation results are compared with the REF-PROP viscosity correlations and experimental data from the ThermoData Engine (TDE) database [52]. Tabulated simulation values are provided in Section SI.VIII of Supporting Information.

3.1. Saturated Liquid

3.1.1. Normal alkanes

Figure 1 compares the ethane results for saturated liquid viscosities obtained with the TraPPE, TraPPE-2, TAMie, Potoff, and AUA4 force fields. As the remainder of this section demonstrates, the over estimation of ethane $\eta_{\text{liq}}^{\text{sat}}$ by Potoff and TAMie is actually an anomaly compared with other normal and branched alkanes. It is not uncommon for the smallest compounds in a homologous series, i.e., methane and ethane, to follow a different trend than the larger compounds. However, the relative magnitudes of $\eta_{\text{liq}}^{\text{sat}}$ for the different force fields are consistent with other compounds, namely, TraPPE and AUA4 viscosities are less than those of TAMie which are less than the Potoff viscosities. This

is expected considering the respective values of λ (the repulsive exponent), i.e., $\lambda = 12$ for TraPPE, TraPPE-2, and AUA4, $\lambda = 14$ for TAMie, and $\lambda = 16$ for Potoff. Note that the TraPPE results are similar to the TraPPE-2 and AUA4 results. Therefore, although the anisotropic CH_3-CH_3 bond provides considerable improvement in simultaneously reproducing vapor-liquid coexistence densities and pressure, it does not appear to significantly improve the viscosity estimates for ethane.

Figure 2 compares the TraPPE, Potoff, and TAMie saturated liquid viscosities for propane, n-butane, and n-octane. Similar to what has been demonstrated in previous studies, the TraPPE force field significantly under estimates $\eta_{\mathrm{liq}}^{\mathrm{sat}}$ (between 30 and 80 %) with the deviation increasing with decreasing temperature [25, 9]. By contrast, the Potoff and TAMie force fields agree with the REFPROP values for these compounds to within 10 %. Although TAMie deviations for propane increase to approximately 50 % at the triple point temperature, Potoff deviations are nearly constant over the entire temperature range studied for each compound.

Figure 3 compares the TraPPE, Potoff, and TAMie saturated liquid viscosities for n-dodecane, n-hexadecane, and n-docosane. The TraPPE percent deviations for these compounds are similar to those observed in Figure 2 for smaller n-alkanes. However, TAMie and Potoff percent deviations demonstrate a stronger temperature dependence for these larger n-alkanes, i.e., the percent deviations increase with decreasing temperature. Although the cause of this trend is unclear, Section 4 suggests that the cut-off distance impacts these larger compounds more than smaller compounds, especially at lower T^{sat}.

3.1.2. Branched alkanes

Figures 4 and 5 compare $\eta_{\mathrm{liq}}^{\mathrm{sat}}$ for branched alkanes. Figures 4 and 5 present results for the compounds classified by Potoff as "short" and "long", respectively [16]. Specifically, Figure 4 depicts 2-methylpropane, 2,2-dimethylpropane, 2-methylbutane, and 2,3-dimethylbutane, while Figure 5 contains 2-methylpentane, 3-methylpentane, and 2,2,4-trimethylpentane. As explained previously, each compound is simulated using the TraPPE and Potoff force fields, 2,2-dimethylpropane and 2,2,4-trimethylpentane are not simulated
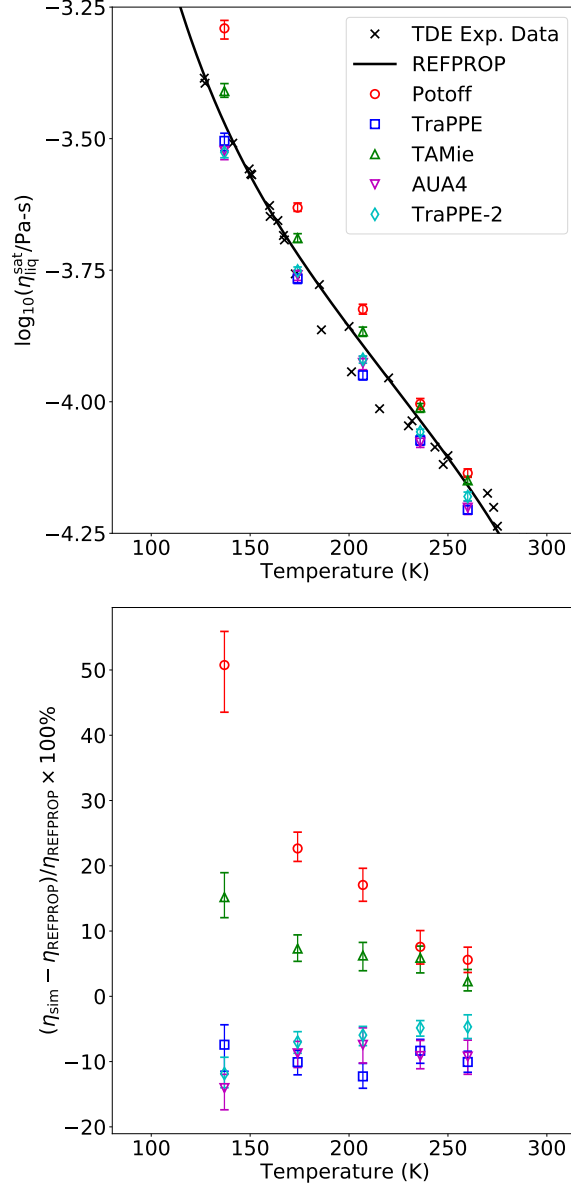
Figure 1: Saturated liquid viscosities for ethane. Top panel compares simulation results with REFPROP correlations and experimental data available in TDE. Bottom panel presents percent deviations between simulated (η_{sim}) and REFPROP (η_{REFPROP}) values. Colors/symbols denote different force fields. Error bars represent the 95 % confidence interval estimated with bootstrap re-sampling. When available, experimental uncertainties are typically smaller than one symbol size. Unless otherwise depicted, REFPROP uncertainties are smaller than the line-width.

16
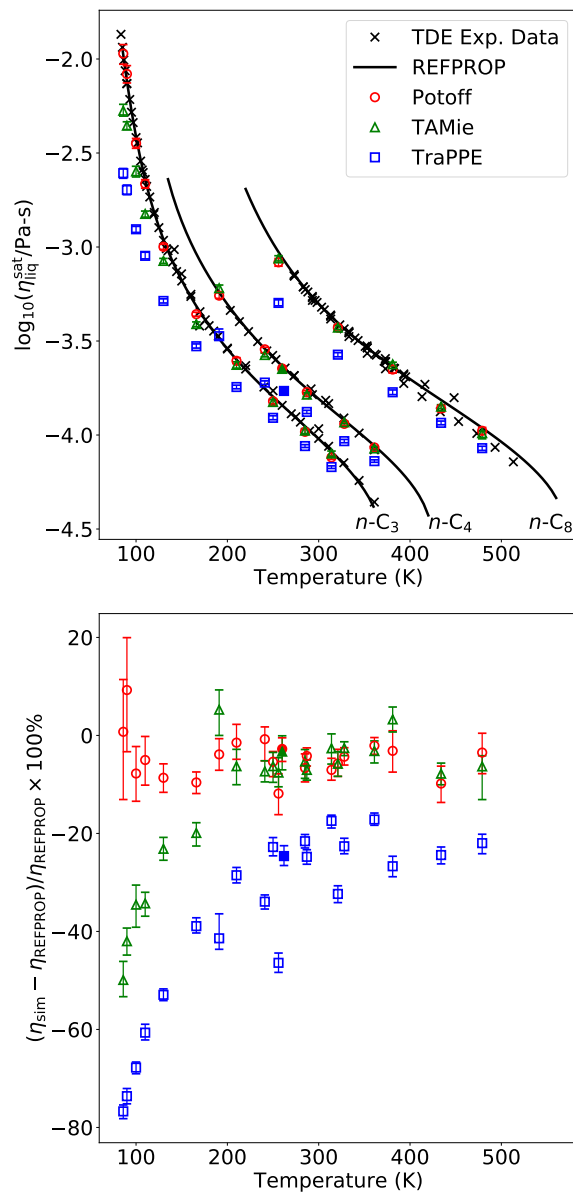
Figure 2: Saturated liquid viscosities for propane (n-C$_3$), n-butane (n-C$_4$), and n-octane (n-C$_8$). See Figure 1 caption for details. Filled symbols correspond to simulations performed at the respective force field $\rho_{\mathrm{liq}}^{\mathrm{sat}}$ (see Section 4).

using TAMie, and only 2,2-dimethylpropane is simulated with AUA4.

From Figures 4 and 5, we see that the Potoff S/L and TAMie force fields are not as accurate for these branched alkanes as for the normal alkanes. In particular, Potoff and TAMie
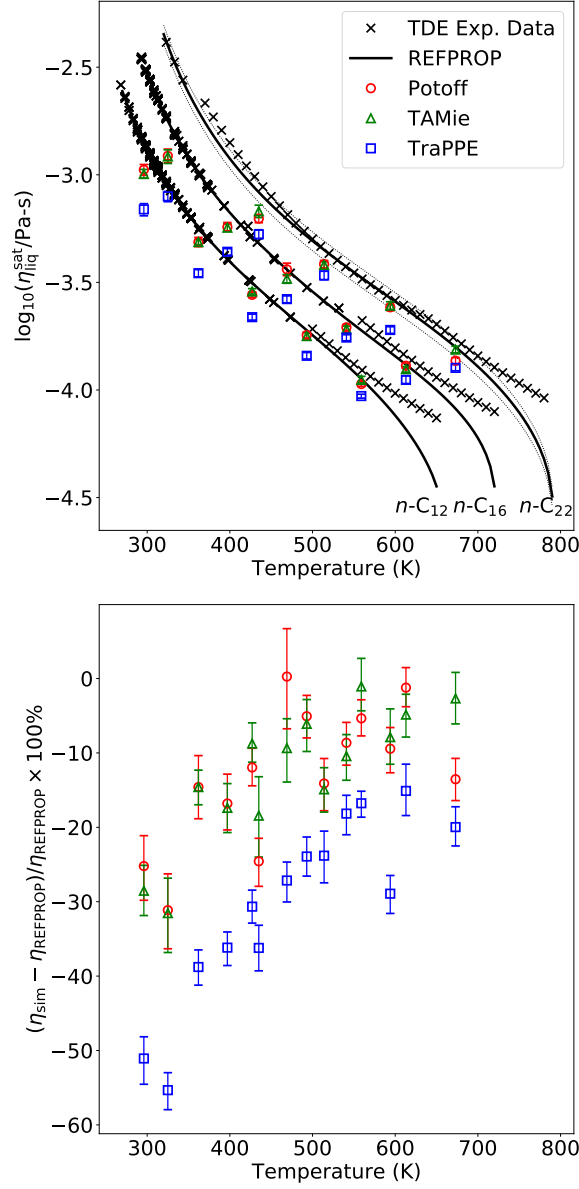
Figure 3: Saturated liquid viscosities for n-dodecane (n-C$_{12}$), n-hexadecane (n-C$_{16}$), and n-docosane (n-C$_{22}$). See Figure 1 caption for details.

deviations demonstrate the same temperature dependence observed for other force fields, where the percent deviations are largest at lower temperatures. However, Potoff still provides considerable improvement compared to the LJ 12-6 based models, i.e., TraPPE and AUA4. Note that the Potoff "short" and "long" parameters in Figures 4 and 5, respec-
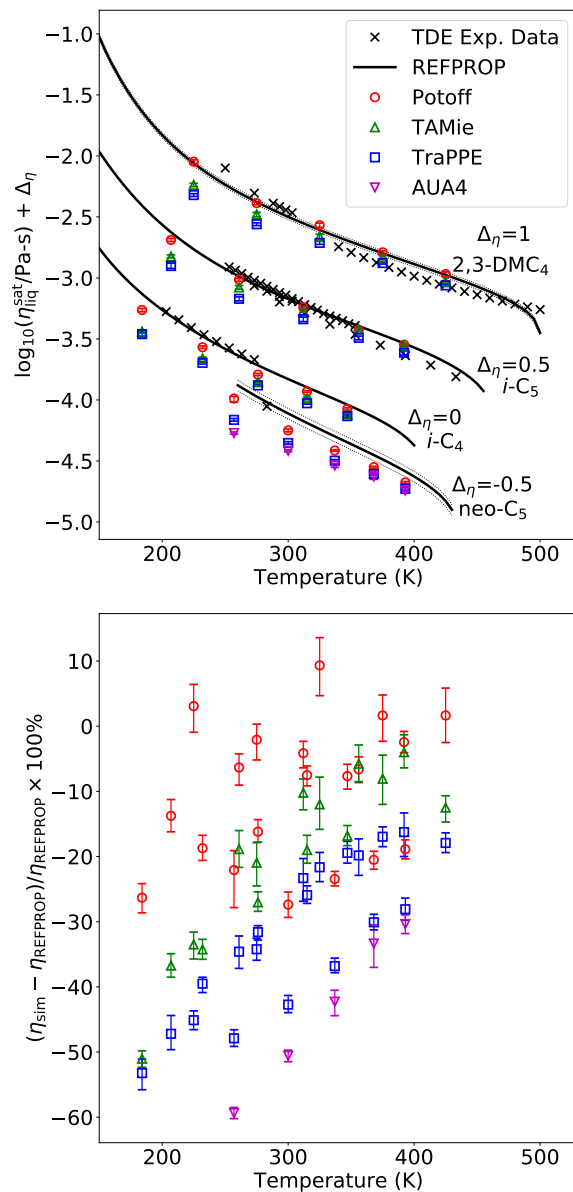
Figure 4: Saturated liquid viscosities for 2-methylpropane (i-C$_4$), 2,2-dimethylpropane (neo-C$_5$), 2-methylbutane (i-C$_5$), and 2,3-dimethylbutane (2,3-DMC$_4$). See Figure 1 caption for details. For clarity, values in top panel are shifted by $\Delta\eta$.

tively, provide similar accuracy.

The deviations for each force field are largest for 2-methylpropane and 2,2-dimethylpropane, the two smallest and most spherical branched alkanes. Since these compounds are pri-
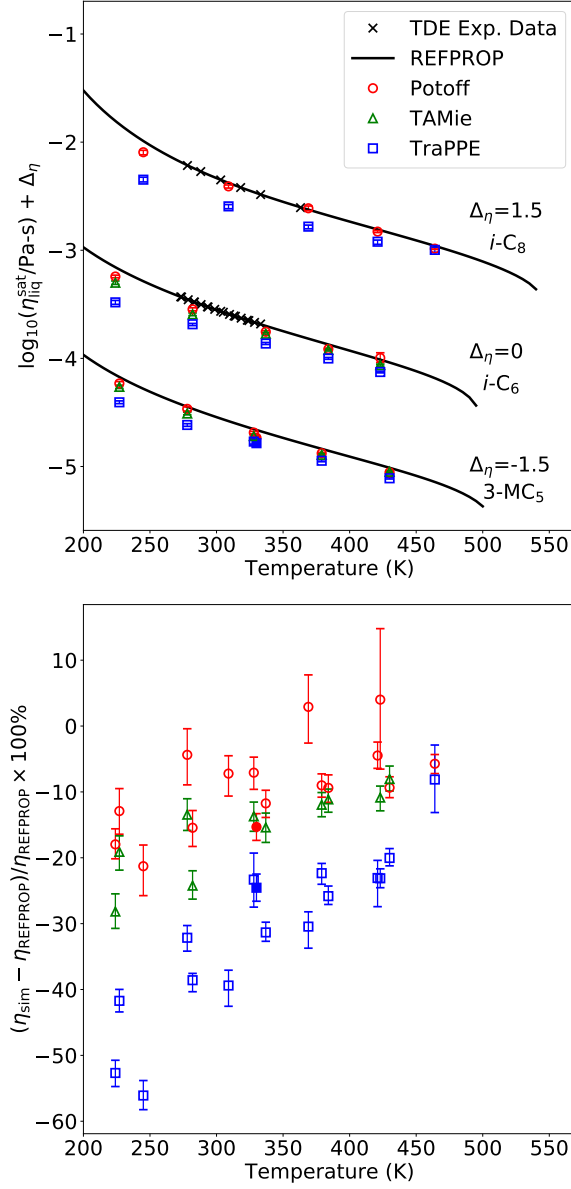
Figure 5: Saturated liquid viscosities for 2-methylpentane (i-C$_6$), 3-methylpentane (3-MC$_5$), and 2,2,4-trimethylpentane (i-C$_8$). See Figure 1 caption for details. For clarity, values in top panel are shifted by $\Delta\eta$. Filled symbols correspond to simulations performed at the respective force field $\rho_{\text{liq}}^{\text{sat}}$ (see Section 4).

marily composed of CH$_3$ UA sites, this poor performance is likely due to the assumption that the CH$_3$ non-bonded parameters are transferable from n-alkanes to branched alkanes. Improvement might be possible if the CH$_3$ parameters were different depending

20

on the neighboring UA site type. However, it is also important to note that the 2,2-dimethylpropane REFPROP viscosity correlation is not considered to be of "reference quality." [3]

3.2. Compressed liquid

Section 3.1 demonstrates that Mie λ-6 based force fields (Potoff and TAMie) are considerably more reliable for predicting saturated liquid viscosities than LJ 12-6 based force fields (TraPPE and AUA4). However, as the Mie λ-6 potential is too repulsive at short distances for $\lambda > 12$, the Potoff (Mie 16-6) and TAMie (Mie 14-6) force fields tend to over estimate pressure at high densities [53]. Since η also increases with larger values of λ, our *ansatz* is that Potoff and TAMie over estimate η at high densities/pressures.

Surprisingly, Gordon shows that a (slightly modified) Mie 14-6 (for CH_3) and Mie 20-6 (for CH_2) potential can accurately predict the η-P dependence for n-hexadecane up to 400 MPa [25]. Since the Gordon force field was parameterized with $\eta_{\text{liq}}^{\text{sat}}$ data, the purpose of this section is to determine if the Potoff and TAMie force fields, which did not include viscosity data in their parameterization, are also reliable for estimating the η-P dependence. To provide additional insight into the consequences of using a Mie λ-6 potential with $\lambda > 12$, we present results for the η-ρ dependence as well (which was not reported by Gordon).

3.2.1. Normal alkanes

Figures 6, 7, and 8 present the compressed liquid viscosities ($\eta_{\text{liq}}^{\text{comp}}$) for propane, n-butane, and n-octane, respectively. Each compound is simulated using the TraPPE, Potoff, and TAMie force fields at various densities. Simulation results are compared with REFPROP correlations and experimental data, when available in TDE.

Figures 6, 7, and 8 demonstrate that the TraPPE force field has a constant negative bias even with increasing density/pressure. The TAMie force field has the most accurate η-ρ dependence, i.e., the error does not increase significantly with respect to density. By contrast, the Potoff potential demonstrates considerable over estimation of η at high

21

densities, which is likely attributed to the overly repulsive Mie 16-6 potential at close distances. Remarkably, the Potoff force field is the most accurate at predicting the η-P dependence from saturation to elevated pressures (approaching 1000 MPa). This can be explained as a cancellation of errors since the Potoff force field significantly over predicts both η and P at high densities. Note that the increase in Potoff deviations for the two highest pressures in Figure 6 can potentially be explained by the large uncertainty in the REFPROP correlation and dubious extrapolation at these extreme pressures. Therefore, although Potoff should not be used to estimate the η-ρ dependence, we conclude that it is the most reliable force field for estimating the η-P dependence.
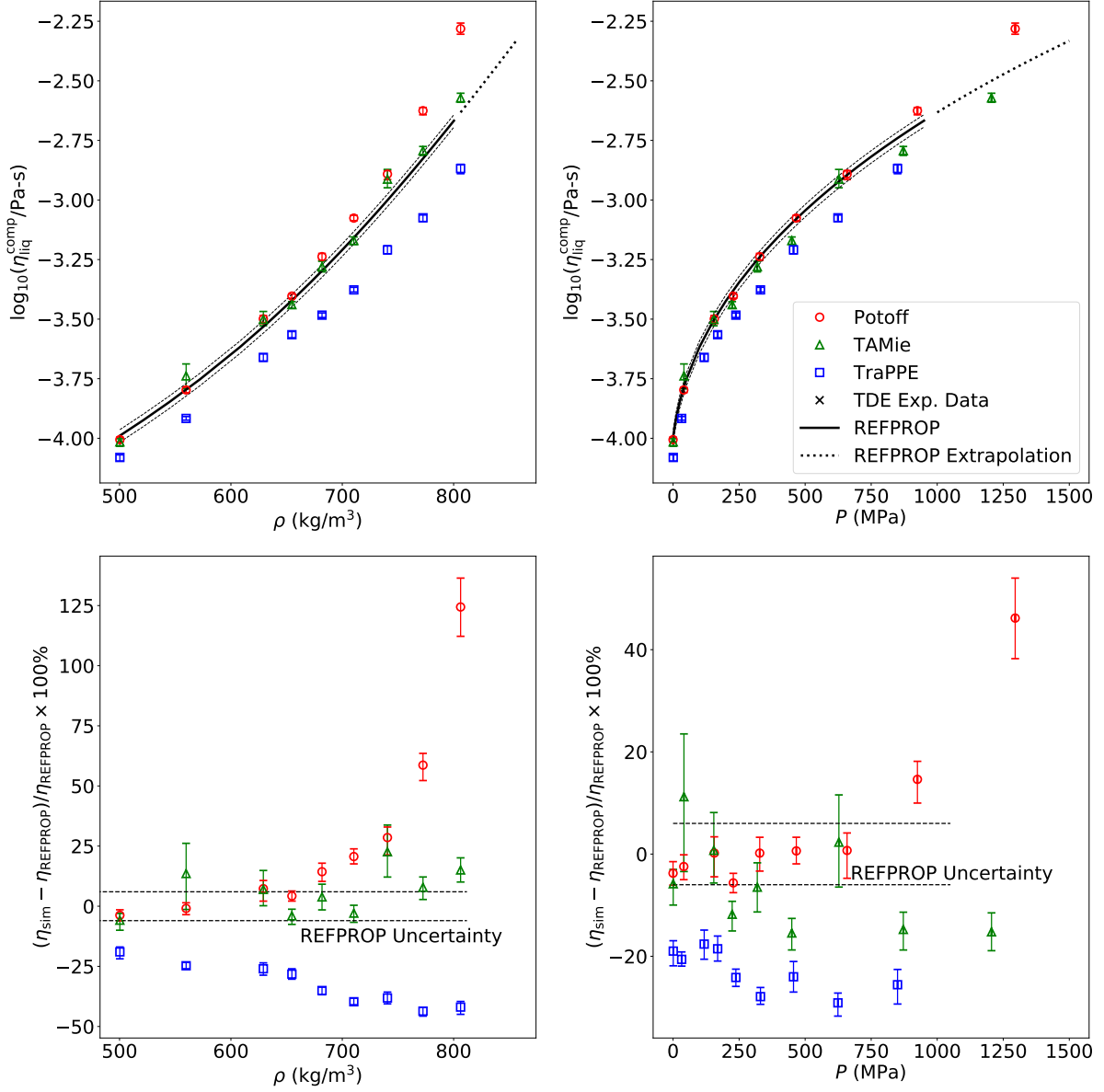
Figure 6: Compressed liquid viscosities at 293 K for propane. Top panels provide η-ρ and η-P dependence. Bottom panels present percent deviations between simulated (η_{sim}) and REFPROP [3] (η_{REFPROP}) values with respect to ρ and P. Experimental data for temperatures between 288 and 298 K are depicted when available in TDE [52]. Dashed lines correspond to reported REFPROP uncertainties. Dotted lines are extrapolation values outside of "reference quality" range, intended to guide the eye when comparing with simulation results at high densities/pressures. Colors/symbols denote different force fields and experimental data. Error bars represent the 95 % confidence interval estimated with bootstrap re-sampling.
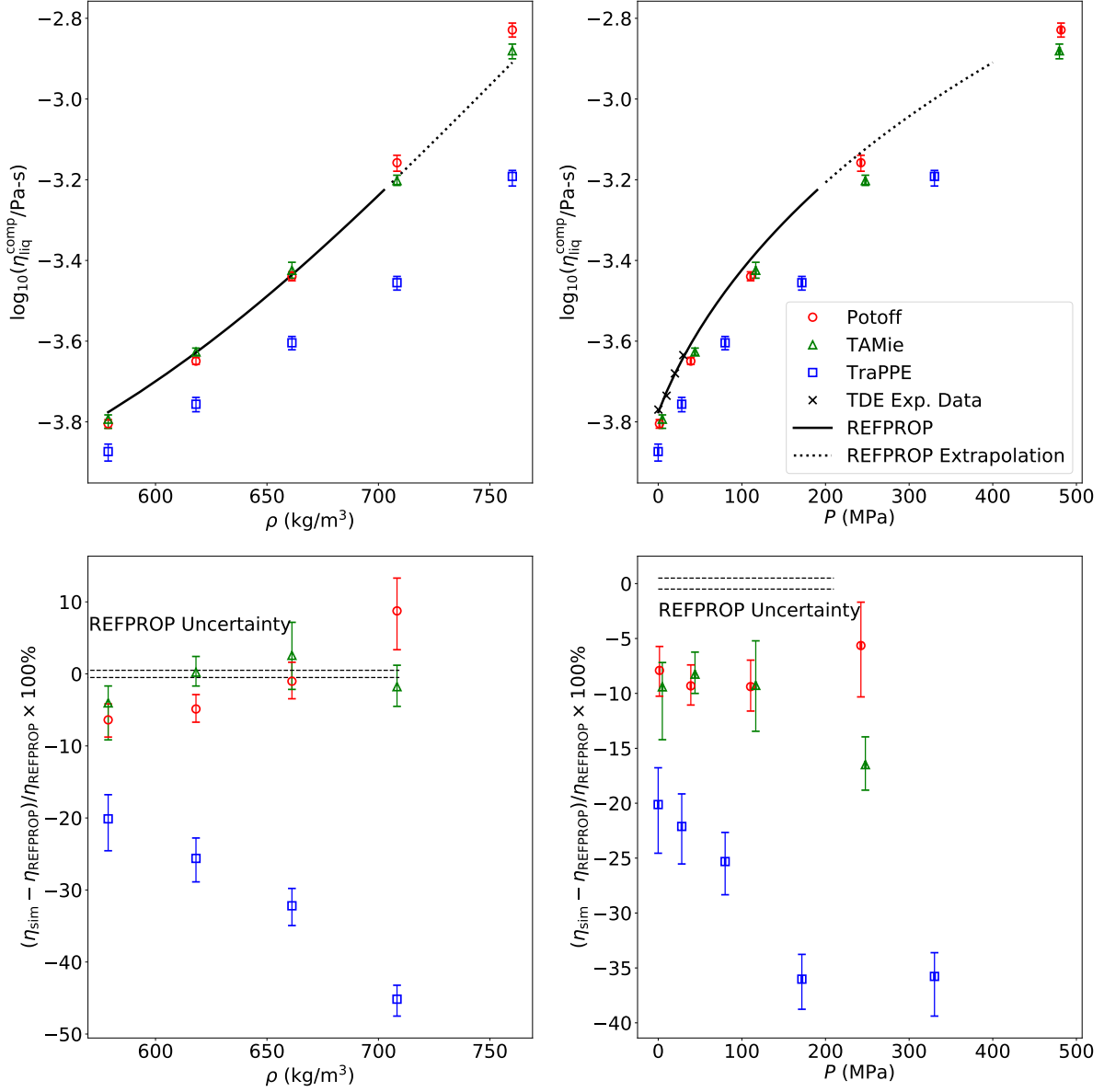
Figure 7: Compressed liquid viscosities at 293 K for *n*-butane. See Figure 6 caption for details.

3.2.2. Branched alkanes

The trends observed in Figures 9 to 12 for branched alkanes are consistent with the compressed liquid trends for *n*-alkanes. Specifically, TraPPE under predicts η with respect to both ρ and P. Potoff over predicts η with respect to ρ but provides a reasonable estimate of the η-P trend. However, as observed in Section 3.1 for $\eta_{\text{liq}}^{\text{sat}}$, Potoff and
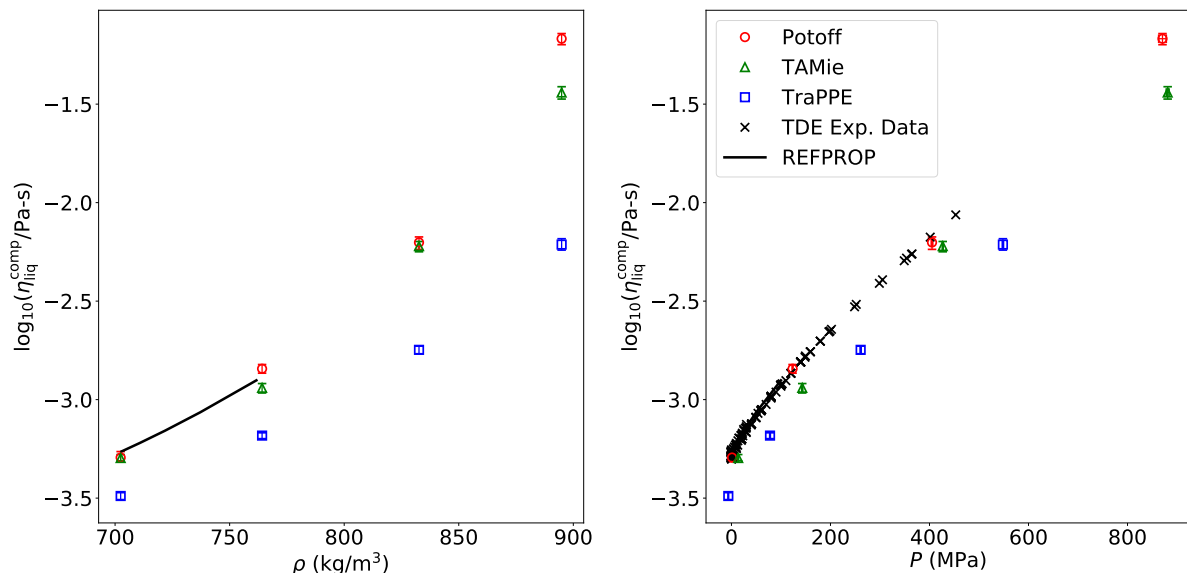
Figure 8: Compressed liquid viscosities at 293 K for *n*-octane. See Figure 6 caption for details.

TAMie are less accurate for branched alkanes than for *n*-alkanes. In particular, the Potoff η-P trends are systematically lower than the REFPROP correlations for 2-methylbutane and 3-methylpentane. However, note that the Potoff η-P trends are quite reliable for 2-methylpropane and 2,2,4-trimethylpentane. These results cannot be attributed to the "short" or "long" parameter distinction, since 2-methylbutane and 2-methylpropane both use "short" parameters while 3-methylpentane and 2,2,4-trimethylpentane both use "long" parameters.

4. Discussion/Limitations

4.1. Liquid structure

While the Potoff force field significantly over predicts $\eta_{\mathrm{liq}}^{\mathrm{comp}}$ at high densities and $T = 293$ K, it does not over predict $\eta_{\mathrm{liq}}^{\mathrm{sat}}$ for the highest saturated liquid densities (those near the triple point temperature) (cf. Figures 2 and 6 for propane). To better understand this seemingly inconsistent result, Figure 13 compares the radial distribution functions (RDF) for the Potoff, TAMie, and TraPPE force fields at three different state points, namely, near
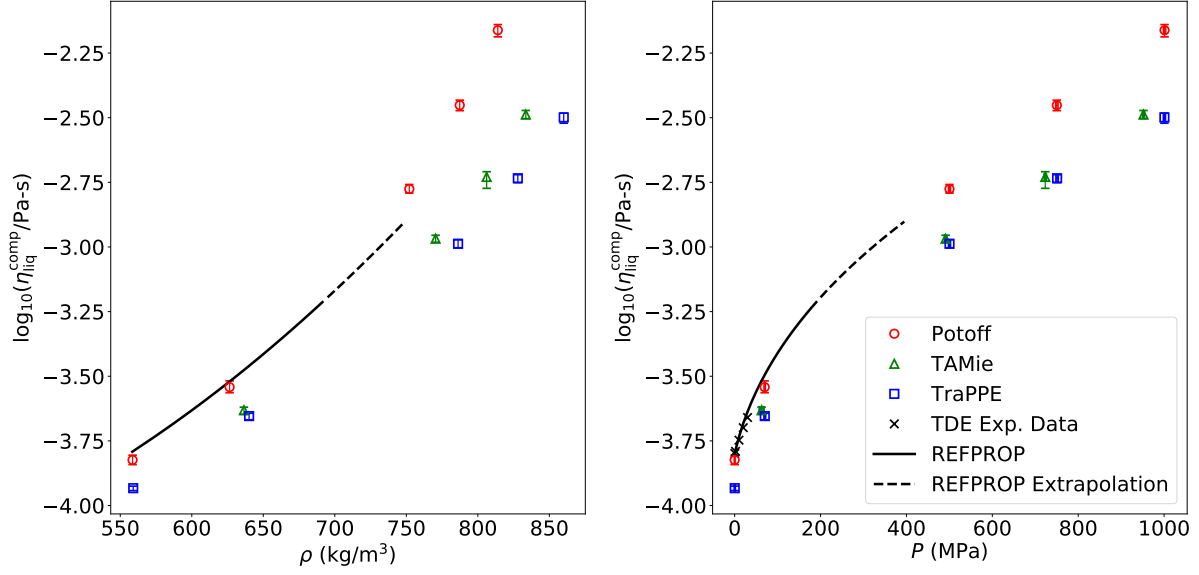
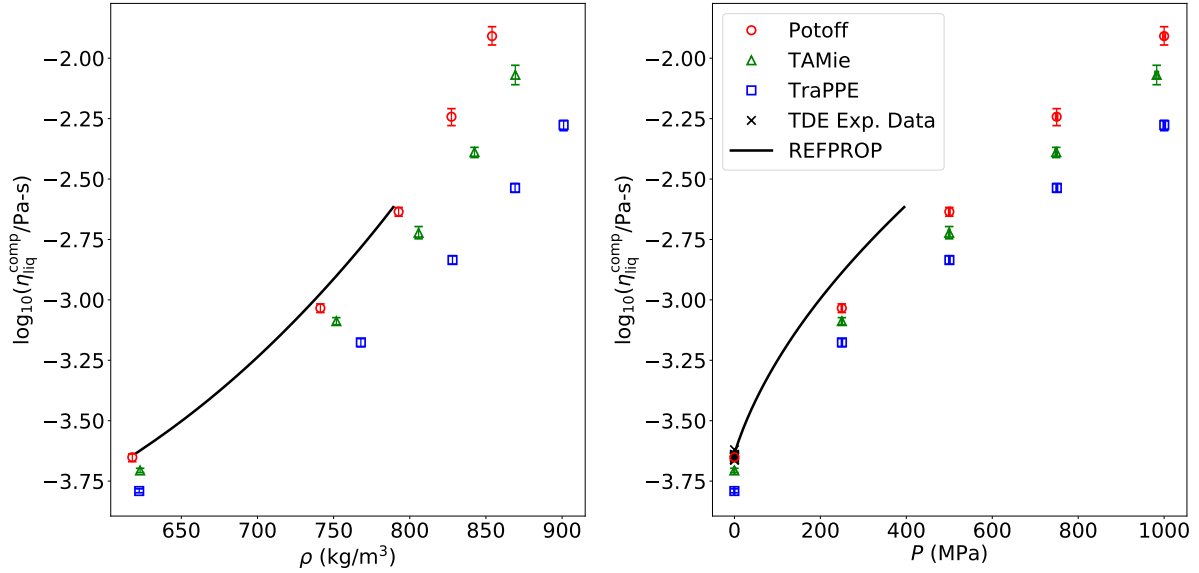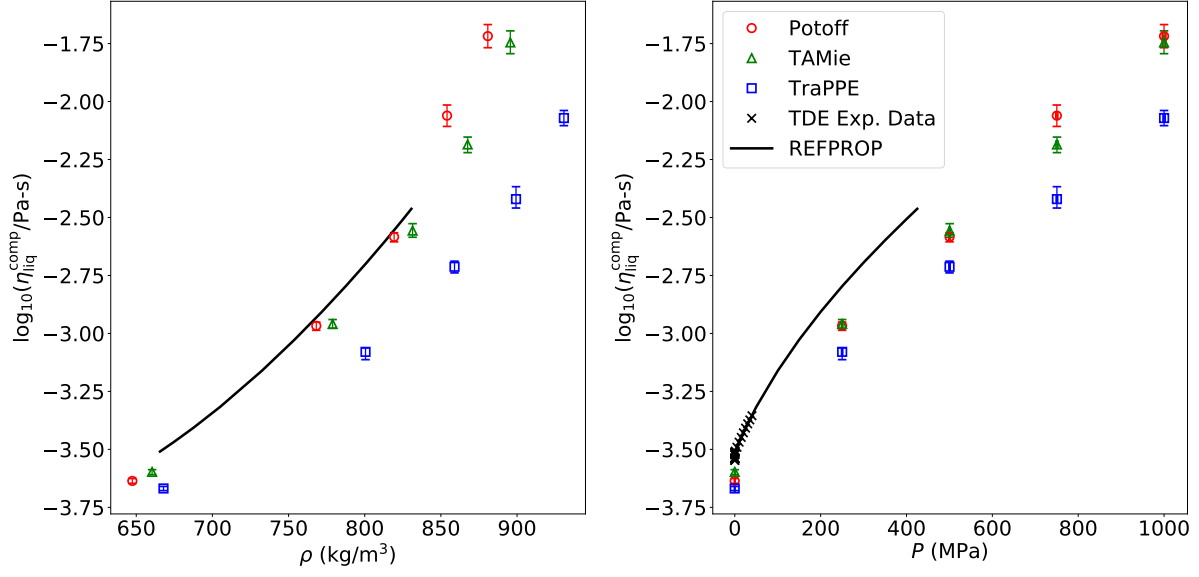Figure 9: Compressed liquid viscosities at 293 K for 2-methylpropane. See Figure 6 caption for details.

Figure 10: Compressed liquid viscosities at 293 K for 2-methylbutane. See Figure 6 caption for details.

the triple point ($T = 86$ K and $\rho = 732.63$ kg/m^3) and two densities along the $T = 293$ K isotherm ($\rho = 732.63$ kg/m^3 and $\rho = 806.23$ kg/m^3). In order to provide a fair comparison between force fields, the RDF is plotted with respect to a reduced distance, namely, r/r_{min}.

Figure 11: Compressed liquid viscosities at 293 K for 3-methylpentane. See Figure 6 caption for details.
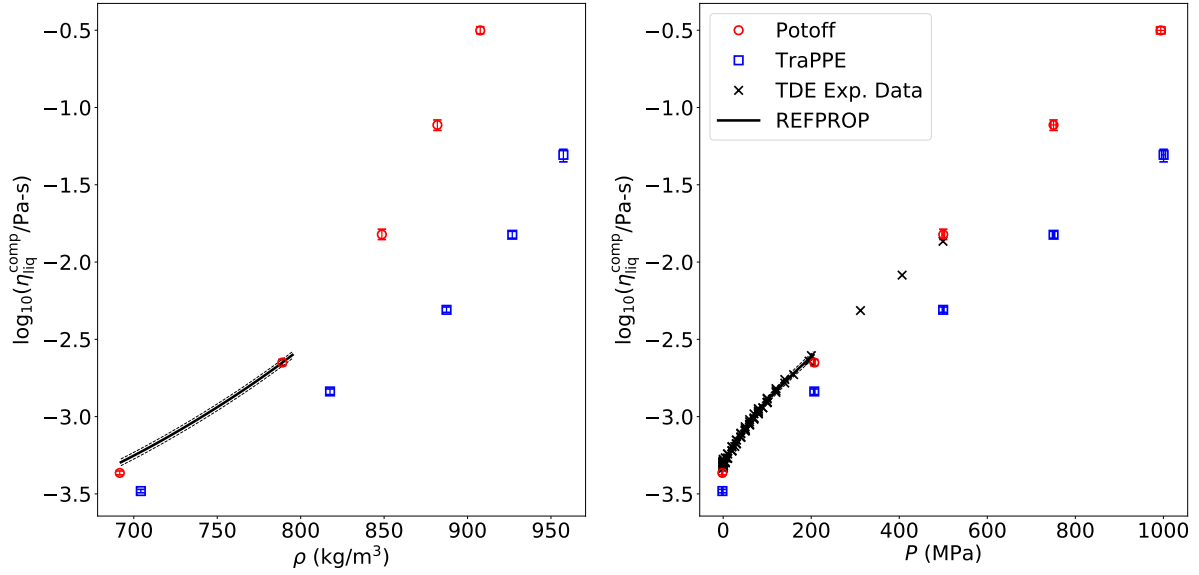

Figure 12: Compressed liquid viscosities at 293 K for 2,2,4-trimethylpentane. See Figure 6 caption for details.

The top panel of Figure 13 demonstrates that the RDF shifts to the left (closer interactions) when increasing the temperature from 86 K to 293 K at $\rho = 732.63$ kg/m^3. Al-
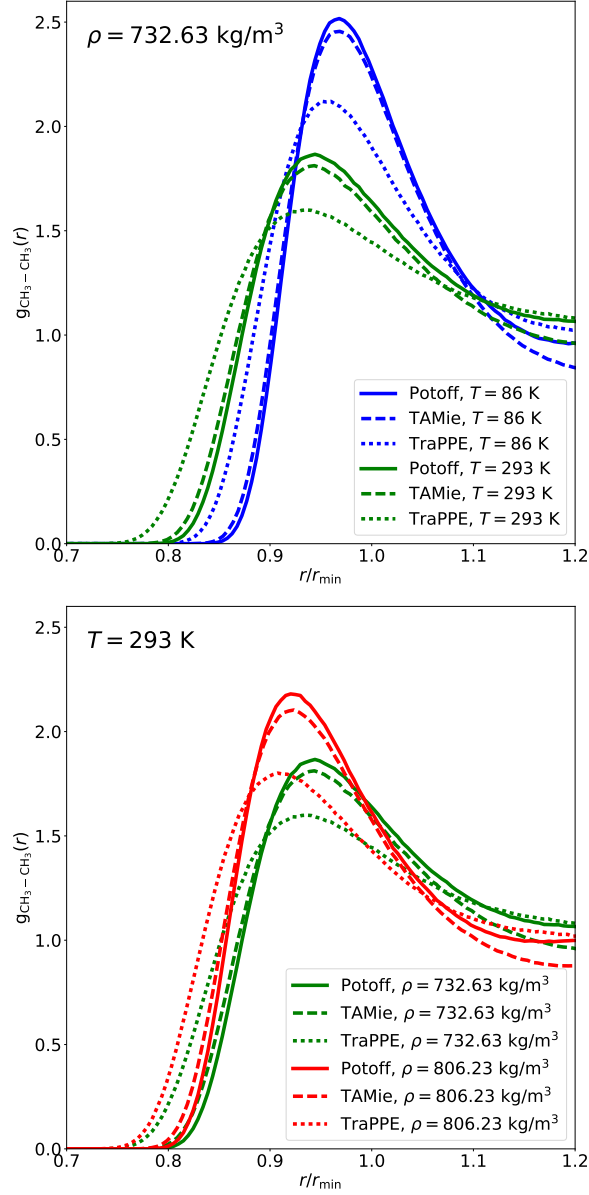
Figure 13: Comparison of radial distribution functions for CH_3-CH_3 interactions ($g_{CH_3-CH_3}(r)$). The top panel compares two different temperatures along the triple point isochore. The bottom panel compares two different densities along the 293 K isotherm. Colors correspond to different state points while line styles denote different force fields.

though the magnitude of this shift is similar for all three force fields, the Potoff viscosities appear to be impacted the most due to the steepness of the Mie 16-6 potential. By contrast, the bottom panel demonstrates that increasing the density at constant temperature

(293 K) does not shift the RDF, although it does increase the frequency of close-range interactions. Therefore, the overly repulsive Mie 16-6 potential is only problematic at high densities if there is sufficient thermal energy for the system to sample extremely close-range interactions. This explains why the Potoff force field is reliable near the triple point but significantly over estimates η for high density systems at 293 K.

4.2. Finite-size effects

Although finite-size effects are often assumed to be negligible for viscosity estimates with equilibrium molecular dynamics, we validate this assumption by plotting η with respect to $N^{-1/3}$ [8]. Figure 14 compares simulation results for 100, 200, 400, and 800 molecule systems. While Figure 14 only presents results for propane, we also observe similar results for a larger compound, specifically, 2,2,4-trimethylpentane.
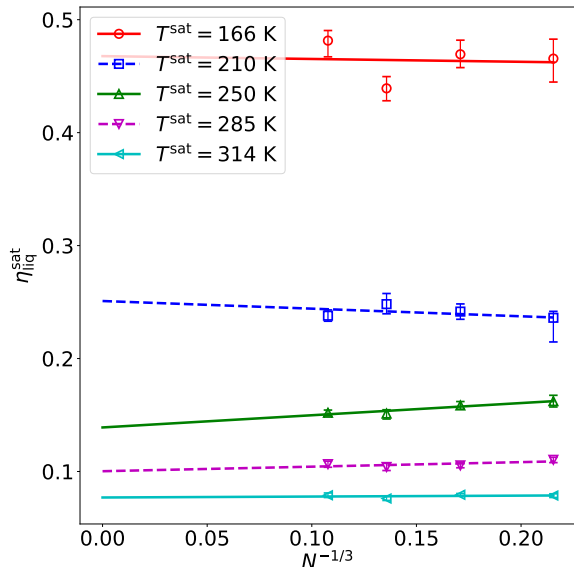

Figure 14: Finite-size effects. Simulation results were obtained for propane with the Potoff force field and $N = 100, 200, 400$, and 800. Colors/symbols denote different saturation temperatures. The lines are obtained from a weighted linear fit with respect to $N^{-1/3}$.

Notice that the averages and uncertainties in Figure 14 are typically quite similar for the different values of N, although some clear exceptions exist, e.g., $N = 800$ and $N = 400$

for $T = 166$ K. The small fluctuations in $\eta_{\text{liq}}^{\text{sat}}$ with respect to $N^{-1/3}$ for dense systems are consistent with the recent findings of Kim et al. [54]. Due to these oscillations, extrapolating to $N^{-1/3} \to 0$, i.e., $N \to \infty$, can result in unrealistic estimates of η. For this reason, we do not recommend the linear fit and extrapolation approach to correct for finite-size effects.

4.3. Cut-off distance

Viscosity, like many other properties, is highly sensitive to the treatment of long-range tail corrections [55]. Furthermore, this section shows that the choice of cut-off distance is also a subtle but important decision. The results presented previously implement a 1.4 nm cut-off for TraPPE, TraPPE-2, and TAMie but a 1.0 nm cut-off for Potoff, as these are the cut-off lengths implemented by the respective authors. Note that the AUA4 developers utilize cut-off distances of 1.0 nm [18, 9, 56], 1.2 nm [19], and equal to half the box length [57, 58] (which is typically larger than 1.4 nm for the systems studied). For simplicity, our AUA4 results are obtained using a 1.4 nm cut-off.

To determine the impact of the cut-off on viscosity estimates, we also perform simulations with the Potoff force field using three different cut-off distances. Specifically, Figure 15 presents the Potoff $\eta_{\text{liq}}^{\text{sat}}$ values for *n*-butane, *n*-octane, and *n*-dodecane using cut-offs of 1.0 nm, 1.4 nm, and 1.8 nm.

Figure 15 demonstrates that for smaller compounds (*n*-butane and *n*-octane) the impact of cut-off is negligible. For larger compounds, however, such as *n*-dodecane, a 1.0 nm cut-off leads to significant error. Unfortunately, Figure 15 demonstrates that even the 1.4 nm cut-off results are not identical to those with a 1.8 nm cut-off for *n*-dodecane.

Recall in Figure 3 that the longer *n*-alkanes demonstrate a temperature-dependent deviation for the Potoff (and TAMie) force field, which was not observed for smaller compounds. Based on the results in Figure 15, we propose that this deviation is not a limitation in the force field, but rather is an artifact of the cut-off length. This is somewhat troubling, since the computationally expensive operation of computing pair interactions is proportional to the square of the cut-off. For example, the 1.8 nm cut-off increases the
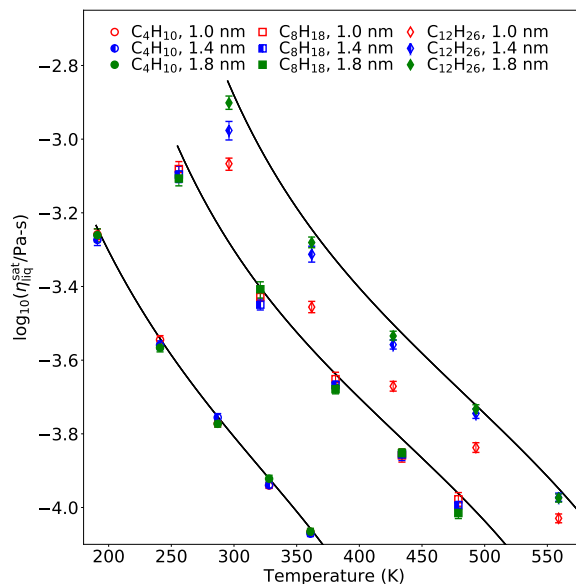
Figure 15: Impact of cut-off distance. Colors/symbols denote different cut-off lengths. Different shapes correspond to *n*-butane, *n*-octane, and *n*-dodecane. REFPROP values are provided as lines for visual reference. Simulations are performed with Potoff force field at saturation conditions.

simulation wall-time for these systems by nearly a factor of two compared to the 1.4 nm cut-off.

In addition, *n*-hexadecane and *n*-docosane were unstable with a 1.0 nm cut-off and a 2 fs time-step. Reducing the time step to 1 fs was capable of stabilizing the 1.0 nm cut-off, but would require twice the computational time and does not necessarily resolve the observed bias. As a compromise between stability, speed, and accuracy, the Potoff results for *n*-dodecane, *n*-hexadecane, and *n*-docosane presented previously in Figure 3 were actually obtained using a 1.4 nm cut-off.

The instability of a 1.0 nm cut-off (with 2 fs time-steps) and the discrepancy in η values obtained with different cut-offs demonstrate the importance of verifying that the cut-off distance is long enough to not impact the system dynamics. Furthermore, this demonstrates a scenario where alternative tail modifications may be preferable, e.g., force-shift or switch-force [29]. Unfortunately, these tail modifications significantly impact thermophysical properties, suggesting that the non-bonded parameters must be re-optimized

31

with the tail modification [59, 60]. Therefore, performing simulations with a force-shift or switch-force potential for Potoff, TraPPE, TAMie, and AUA4 would likely result in inaccurate viscosities. Re-parameterizing the non-bonded interactions for a force-shift or switch-force potential is beyond the scope of this study.

4.4. REFPROP $\rho_{\text{liq}}^{\text{sat}}$ vs. force field $\rho_{\text{liq}}^{\text{sat}}$

The use of REFPROP $\rho_{\text{liq}}^{\text{sat}}$ instead of the force field $\rho_{\text{liq}}^{\text{sat}}$ can lead to meta-stable simulations and spurious results. This occurs when the force field $P_{\text{vap}}^{\text{sat}}$ is less than the REFPROP $P_{\text{vap}}^{\text{sat}}$. Fortunately, this is uncommon since Potoff, TAMie, AUA4, and TraPPE-2 are quite reliable for estimating $P_{\text{vap}}^{\text{sat}}$ and TraPPE significantly over estimates $P_{\text{vap}}^{\text{sat}}$. Furthermore, it is important that the force field melting point is below the simulation T^{sat}. This does not appear to be an issue, however, since the RDFs for each force field are liquid-like even for the propane simulations near the triple point temperature (cf. top panel of Figure 13).

There are at least four reasons why we perform simulations at the REFPROP $\rho_{\text{liq}}^{\text{sat}}$ instead of the force field $\rho_{\text{liq}}^{\text{sat}}$. First, this approach allows for a fair comparison of the force fields' ability to predict viscosity, without penalizing force fields which are less accurate at predicting $\rho_{\text{liq}}^{\text{sat}}$ or rewarding force fields that mask their deficiencies in predicting viscosity by over- or under estimating $\rho_{\text{liq}}^{\text{sat}}$. Second, this facilitates comparing force fields over the entire range of saturation temperatures, whereas this is extremely challenging using standard simulation methods for determining vapor-liquid saturation densities, such as Gibbs Ensemble Monte Carlo (GEMC) or Grand Canonical Monte Carlo (GCMC) histogram reweighting (HR). Third, it is straightforward, at least qualitatively, to account for a systematic deviation between the force field and REFPROP $\rho_{\text{liq}}^{\text{sat}}$, e.g., a positive bias in $\rho_{\text{liq}}^{\text{sat}}$ will increase $\eta_{\text{liq}}^{\text{sat}}$. Fourth, since each of the studied force fields were optimized with $\rho_{\text{liq}}^{\text{sat}}$ data, deviations between the REFPROP and force field densities are small, typically less than 1 % (see Table 1 of Reference 17).

However, due to the exponential dependence of η on ρ, small differences in $\rho_{\text{liq}}^{\text{sat}}$ can result in relatively large deviations in $\eta_{\text{liq}}^{\text{sat}}$. For this reason, we perform a small set of validation simulations to determine the variability caused by utilizing the force field or

REFPROP values for $\rho_{\text{liq}}^{\text{sat}}$. Specifically, we simulate *n*-butane with Potoff, TraPPE, and TAMie and 3-methylpentane with Potoff and TraPPE using the $\rho_{\text{liq}}^{\text{sat}}$ literature values reported for the corresponding force field [12, 16, 17, 14], where Reference 12 utilizes GEMC and References 14, 16, 17 use GCMC-HR.

The results with the "true" force field $\rho_{\text{liq}}^{\text{sat}}$ for *n*-butane and 3-methylpentane are found in Figures 2 and 5, respectively, as filled symbols. Note that the Potoff, TAMie, and TraPPE *n*-butane and TraPPE 3-methylpentane filled points are consistent with the respective empty points. This is due to the good agreement between the force field $\rho_{\text{liq}}^{\text{sat}}$ and the REFPROP $\rho_{\text{liq}}^{\text{sat}}$ (less than 0.3 %). By contrast, the Potoff 3-methylpentane filled point is approximately 3 % lower than the respective empty points. This is because the Potoff force field under estimates $\rho_{\text{liq}}^{\text{sat}}$ by around 1.15 % [17]. In comparison, the Potoff S/L deviations in $\rho_{\text{liq}}^{\text{sat}}$ are between -0.12 % and -0.60 % for all other branched compounds studied. TraPPE deviations in $\rho_{\text{liq}}^{\text{sat}}$ are less than $\pm$ 0.6 % for all compounds except for 2,2-dimethylpropane and 2,2,4-trimethylpentane, which have -1.55 % and 2.81 % deviations, respectively. Therefore, utilizing the actual force field $\rho_{\text{liq}}^{\text{sat}}$ values would not alter the qualitative trends observed in Figures 1 to 5 and should only modify the quantitative values by a few percent in most cases and not more than 10 % in the most extreme cases.

5. Conclusions

This study demonstrates the improvement that has taken place over the past two decades for predicting viscosity with molecular simulation. First, following "Best Practices" for EMD lead to more reproducible results. Second, the state-of-the-art Mie λ-6 force fields are significantly more accurate than the traditional Lennard-Jones 12-6 force fields for viscosity, as well as for vapor-liquid coexistence properties. More specifically, the Potoff and TAMie force fields typically predict saturated liquid viscosities for *n*-alkanes to within 10 % of the REFPROP values. By contrast, the TraPPE and AUA4 models under predict saturated liquid viscosities by 20 % to 50 %, where the deviations are largest at lower temperatures. While Potoff and TAMie are also more reliable for branched alkanes, deviations are larger and demonstrate a similar temperature dependence.

The key limitation of the Potoff force field is that the choice of $\lambda = 16$ is too repulsive at close distances, which causes the viscosity to be over estimated at high densities. Due to a fortuitous cancellation of errors, the Potoff potential does provide a reliable η-P trend. Since TAMie uses $\lambda = 14$, the η-ρ trend is slightly more reliable than that of Potoff. It is important to emphasize that transport properties were not included in the training set for parameterizing the Potoff and TAMie force fields. Therefore, the results from this study demonstrate that the improved prediction of static vapor-liquid coexistence properties obtained with Mie λ-6 potentials also results in improved prediction of a dynamic property, liquid viscosity.

Supporting Information

Section SI.I provides GROMACS input files. Section SI.II enumerates all systems simulated. Section SI.III details the MD integrator, thermostat, and barostat. Section SI.IV compares simulation results with varying production times. Section SI.V determines the sensitivity of our results to the use of fixed bonds. Section SI.VI outlines the Green-Kubo analysis process. Section SI.VII validates our methods by comparing with reference simulation values. Section SI.VIII contains tabulated simulation values.

Partial contribution of NIST, an agency of the United States government; not subject to copyright in the United States.

References

References

[1] M. J. Assael, C. P. Oliveira, M. Papadaki, and W. A. Wakeham. Vibrating-wire viscometers for liquids at high pressures. *International Journal of Thermophysics*, 13(4):593–615, 1992.

[2] Johnny R. Zambrano, Manuel Sobrino, M. Carmen MartÃ■n, Miguel A. Villa-maÃśÃąn, CÃľsar R. Chamorro, and JosÃľ J. Segovia. Contributing to accurate high pressure viscosity measurements: Vibrating wire viscometer and falling body viscometer techniques. *The Journal of Chemical Thermodynamics*, 96:104 – 116, 2016.

[3] E. W. Lemmon, I. H. Bell, M. L. Huber, and M. O. McLinden. NIST Standard Reference Database 23: Reference Fluid Thermodynamic and Transport Properties-REFPROP, Version 10.0, National Institute of Standards and Technology, 2018.

[4] B.E. Poling, J.M. Prausnitz, and J.P. O'Connell. *The Properties of Gases and Liquids, 5th ed.* McGraw-Hill Companies, Inc., 2001. Chapter 9.

[5] Ángel Mulero, Isidro Cachadiña, and José O. Valderrama. Artificial neural network for the correlation and prediction of surface tension of refrigerants. *Fluid Phase Equilibria*, 451:60 – 67, 2017.

[6] Seongmin Lee, Kiho Park, Yunkyung Kwon, Tae-Yun Park, and Dae Ryook Yang. A modified scaled variable reduced coordinate (SVRC)-quantitative structure property relationship (QSPR) model for predicting liquid viscosity of pure organic compounds. *Korean Journal of Chemical Engineering*, 34(10):2715–2724, 2017.

[7] Oliver Lötgering-Lin and Joachim Gross. Group contribution method for viscosities based on entropy scaling using the perturbed-chain polar statistical associating fluid theory. *Industrial & Engineering Chemistry Research*, 54(32):7942–7952, 2015.

[8] Edward J. Maginn, Richard A. Messerly, Daniel J. Carlson, Daniel R. Roe, and J. Richard Elliott. Best practices for computing transport properties 1. Self-diffusivity and viscosity from equilibrium molecular dynamics v1. *Living Journal of Computational Molecular Science*, Pending publication, 2018.

[9] Carlos Nieto-Draghi, Philippe Ungerer, and Bernard Rousseau. Optimization of the anisotropic united atoms intermolecular potential for *n*-alkanes: Improvement of transport properties. *The Journal of Chemical Physics*, 125(4):044517, 2006.

[10] Damien A. Bernard-Brunel and Jeffrey J. Potoff. Effect of torsional potential on the predicted phase behavior of *n*-alkanes. *Fluid Phase Equilibria*, 279(2):100 – 104, 2009.

[11] M. G. Martin and J. I. Siepmann. Transferable potentials for phase equilibria. 1. United-atom description of *n*-alkanes. *The Journal of Physical Chemistry B*, 102(14):2569–2577, 1998.

[12] Marcus G. Martin and J. Ilja Siepmann. Novel configurational-bias monte carlo method for branched molecules. Transferable Potentials for Phase Equilibria. 2. United-Atom Description of Branched Alkanes. *The Journal of Physical Chemistry B*, 103(21):4508–4517, 1999.

[13] Mansi S. Shah, J. Ilja Siepmann, and Michael Tsapatsis. Transferable potentials for phase equilibria. Improved united-atom description of ethane and ethylene. *AIChE Journal*, 63(11):5098–5110, 2017.

[14] Andrea Hemmen and Joachim Gross. Transferable anisotropic united-atom force field based on the Mie potential for phase equilibrium calculations: *n*-alkanes and *n*-olefins. *The Journal of Physical Chemistry B*, 119(35):11695–11707, 2015.

[15] Dominik Weidler and Joachim Gross. Transferable anisotropic united-atom force field based on the Mie potential for phase equilibria: Aldehydes, ketones, and small cyclic alkanes. *Industrial & Engineering Chemistry Research*, 55(46):12123–12132, 2016.

[16] J. J. Potoff and D. A. Bernard-Brunel. Mie potentials for phase equilibria calculations: Applications to alkanes and perfluoroalkanes. *The Journal of Physical Chemistry B*, 113(44):14725–14731, 2009.

[17] Jason R. Mick, Mohammad Soroush Barhaghi, Brock Jackman, Loren Schwiebert, and Jeffrey J. Potoff. Optimized Mie potentials for phase equilibria: Application to branched alkanes. *Journal of Chemical & Engineering Data*, 62(6):1806–1818, 2017.

[18] Philippe Ungerer, Christele Beauvais, Jerome Delhommelle, Anne Boutin, Bernard Rousseau, and Alain H. Fuchs. Optimization of the anisotropic united atoms intermolecular potential for *n*-alkanes. *The Journal of Chemical Physics*, 112(12):5499–5510, 2000.

[19] Carlos Nieto-Draghi, Anthony Bocahut, Benoît Creton, Pascal Have, Aziz Ghoufi, Aurélie Wender, , Anne Boutin, Bernard Rousseau, and Laurent Normand. Optimisation of the dynamical behaviour of the anisotropic united atom model of branched alkanes: application to the molecular simulation of fuel gasoline. *Molecular Simulation*, 34(2):211–230, 2008.

[20] William Allen and Richard L. Rowley. Predicting the viscosity of alkanes using nonequilibrium molecular dynamics: Evaluation of intermolecular potential models. *The Journal of Chemical Physics*, 106(24):10273–10281, 1997.

[21] Rajdeep Singh Payal, S. Balasubramanian, Indranil Rudra, Kunj Tandon, Ingo Mahlke, David Doyle, and Roger Cracknell. Shear viscosity of linear alkanes through molecular simulations: quantitative tests for *n*-decane and *n*-hexadecane. *Molecular Simulation*, 38(14-15):1234–1241, 2012.

[22] Maurizio Mondello and Gary S. Grest. Viscosity calculations of *n*-alkanes by equilibrium molecular dynamics. *The Journal of Chemical Physics*, 106(22):9327–9336, 1997.

[23] Molecular simulation of the thermophysical properties of fluids: From understanding toward quantitative predictions. *Journal of Molecular Liquids*, 134(1):71 – 89, 2007.

[24] James P Ewen, Chiara Gattinoni, Foram M. Thakkar, Neal Morgan, H A Spikes, and Daniele Dini. A comparison of classical force-fields for molecular dynamics simulations of lubricants. *Materials*, 9(8):651, 2016.

[25] Peter A. Gordon. Development of intermolecular potentials for predicting transport properties of hydrocarbons. *The Journal of Chemical Physics*, 125(1):014504, 2006.

[26] Hai Hoang, Stéphanie Delage-Santacreu, and Guillaume Galliero. Simultaneous description of equilibrium, interfacial, and transport properties of fluids using a Mie chain coarse-grained force field. *Industrial & Engineering Chemistry Research*, 56(32):9213–9226, 2017.

[27] Carmelo Herdes, Tim S. Totton, and Erich A. Müller. Coarse grained force field for the molecular simulation of natural gases and condensates. *Fluid Phase Equilibria*, 406:91 – 100, 2015.

[28] M. P. Allen and D. J. Tildesley. *Computer Simulation of Liquids*. Clarendon Press ; Oxford University Press, Oxford England New York, 1987.

[29] M.J. Abraham, D. van der Spoel, E. Lindahl, B.Hess, and the GROMACS development team. *GROMACS User Manual version 2018, www.gromacs.org (2018)*.

[30] Vince K. Shen, Daniel W. Siderius, William P. Krekelberg, and Harold W. Hatch. NIST standard reference simulation website, NIST standard reference database number 173. *National Institute of Standards and Technology*, Gaithersburg MD, 20899. https://www.nist.gov/programs-projects/nist-standard-reference-simulation-website. Retrieved July 27, 2018.

[31] Loukas I. Kioupis and Edward J. Maginn. Impact of molecular architecture on the high-pressure rheology of hydrocarbon fluids. *The Journal of Physical Chemistry B*, 104(32):7774–7783, 2000.

[32] Berk Hess, Henk Bekker, Herman J. C. Berendsen, and Johannes G. E. M. Fraaije. LINCS: A linear constraint solver for molecular simulations. *Journal of Computational Chemistry*, 18(12):1463–1472, 1998.

[33] Berk Hess. P-LINCS: A parallel linear constraint solver for molecular simulation. *Journal of Chemical Theory and Computation*, 4(1):116–122, 2008.

[34] Yong Zhang, Akihito Otani, and Edward J. Maginn. Reliable viscosity calculation from equilibrium molecular dynamics simulations: A time decomposition method. *Journal of Chemical Theory and Computation*, 11(8):3537–3546, 2015.

[35] D. Bücker and W. Wagner. A reference equation of state for the thermodynamic properties of ethane for temperatures from the melting line to 675 K and pressures up to 900 MPa. *Journal of Physical and Chemical Reference Data*, 35(1):205–266, 2006.

[36] Eckhard Vogel, Roland Span, and Sebastian Herrmann. Reference correlation for the viscosity of ethane. *Journal of Physical and Chemical Reference Data*, 44(4):043101, 2015.

[37] Eric W. Lemmon, Mark O. McLinden, and Wolfgang Wagner. Thermodynamic properties of propane. iii. a reference equation of state for temperatures from the melting line to 650 K and pressures up to 1000 MPa. *Journal of Chemical & Engineering Data*, 54(12):3141–3180, 2009.

[38] Eckhard Vogel and Sebastian Herrmann. New formulation for the viscosity of propane. *Journal of Physical and Chemical Reference Data*, 45(4):043103, 2016.

[39] D. Bücker and W. Wagner. Reference equations of state for the thermodynamic properties of fluid phase *n*-butane and isobutane. *Journal of Physical and Chemical Reference Data*, 35(2):929–1019, 2006.

[40] Sebastian Herrmann and Eckhard Vogel. New formulation for the viscosity of n-butane. *Journal of Physical and Chemical Reference Data*, 47(1):013104, 2018.

[41] R. Beckmueller, M. Thol, and R. Span. Fundamental equation of state for *n*-octane. *International Journal of Thermophysics*, Pending publication, 2018.

[42] Marcia L. Huber, Arno Laesecke, and Hong Wei Xiang. Viscosity correlations for minor constituent fluids in natural gas: *n*-octane, *n*-nonane and *n*-decane. *Fluid Phase Equilibria*, 224(2):263 – 270, 2004.

[43] Eric W. Lemmon and Marcia L. Huber. Thermodynamic properties of n-dodecane. *Energy & Fuels*, 18(4):960–967, 2004.

[44] Marcia L. Huber, Arno Laesecke, and Richard Perkins. Transport properties of n-dodecane. *Energy & Fuels*, 18(4):968–975, 2004.

[45] R. Romeo and E.W. Lemmon. To be submitted. 2018.

[46] Private communication to M. Huber from V. Vesovic, Oct. 2017.

[47] M.L. Huber. Models for the viscosity, thermal conductivity, and surface tension of selected pure fluids as implemented in REFPROP v10.0. *NISTIR 8209*, Pending publication, 2018.

[48] Eric W. Lemmon and Roland Span. Short fundamental equations of state for 20 industrial fluids. *Journal of Chemical & Engineering Data*, 51(3):785–850, 2006.

[49] E. Vogel, C. Küchenmeister, and E. Bich. Viscosity correlation for isobutane over wide ranges of the fluid region. *International Journal of Thermophysics*, 21(2):343–356, 2000.

[50] K. Gao, J. Wu, and E.W. Lemmon. Unpublished equation. 2017.

[51] T.M. Blackham, A.K. Lemmon, and E.W. Lemmon. Fundamental equation of state for isooctane. *International Journal of Thermophysics*, Pending publication, 2018.

[52] Michael Frenkel, Robert D. Chirico, Vladimir Diky, Xinjian Yan, Qian Dong, and Chris Muzny. Thermodata engine (TDE): software implementation of the dynamic data evaluation concept. *Journal of Chemical Information and Modeling*, 45(4):816–838, 2005.

[53] Richard A. Messerly, Michael R. Shirts, and Andrei F. Kazakov. Uncertainty quantification confirms unreliable extrapolation toward high pressures for united-atom Mie λ-6 force field. *Journal of Chemical Physics*, Pending publication, 2018.

[54] Kang-Sahn Kim, Myung Hoon Han, Changho Kim, Zhen Li, George Em Karniadakis, and Eok Kyun Lee. Nature of intrinsic uncertainties in equilibrium molecular dynamics estimation of shear viscosity for simple and complex fluids. *The Journal of Chemical Physics*, 149(4):044510, 2018.

[55] Alison N. Leonard, Andrew C. Simmonett, Frank C. Pickard, Jing Huang, Richard M. Venable, Jeffery B. Klauda, Bernard R. Brooks, and Richard W. Pastor. Comparison of additive and polarizable models with explicit treatment of long-range lennard-jones interactions using alkane simulations. *Journal of Chemical Theory and Computation*, 14(2):948–958, 2018.

[56] Emeric Bourasseau, Philippe Ungerer, Anne Boutin, and Alain H. Fuchs. Monte carlo simulation of branched alkanes and long chain *n*-alkanes with anisotropic united atoms intermolecular potential. *Molecular Simulation*, 28(4):317–336, 2002.

[57] Emeric Bourasseau, Mehalia Haboudou, Anne Boutin, Alain H. Fuchs, and Philippe Ungerer. New optimization method for intermolecular potentials: Optimization of a new anisotropic united atoms potential for olefins: Prediction of equilibrium properties. *The Journal of Chemical Physics*, 118(7):3020–3034, 2003.

[58] Javier Pérez-Pellitero, Emeric Bourasseau, Isabelle Demachy, Jacqueline Ridard, Philippe Ungerer, and Allan D. Mackie. Anisotropic united-atoms (AUA) potential for alcohols. *The Journal of Physical Chemistry B*, 112(32):9853–9863, 2008.

[59] Monika Thol, Gábor Rutkai, Roland Span, Jadran Vrabec, and Rolf Lustig. Equation of state for the Lennard-Jones truncated and shifted model fluid. *International Journal of Thermophysics*, 36(1):25–43, 2015.

[60] Monika Thol, Gábor Rutkai, Andreas Köster, Rolf Lustig, Roland Span, and Jadran Vrabec. Equation of state for the Lennard-Jones fluid. *Journal of Physical and Chemical Reference Data*, 45(2):023101, 2016.